Physical Properties and Bonding in RE_3TiSb_5 (RE = La, Ce, Pr, Nd, Sm)

S. H. Devon Moore, Laura Deakin, Michael J. Ferguson, and Arthur Mar*

Department of Chemistry, University of Alberta, Edmonton, Alberta, Canada T6G 2G2

Received July 10, 2002. Revised Manuscript Received September 11, 2002

Electrical transport and magnetic properties have been measured for the family of ternary rare-earth transition-metal antimonides RE_3TiSb_5 (RE = La, Ce, Pr, Nd, Sm). Single-crystal X-ray structures have now been determined for all members of this series. All are metallic, with anomalies appearing in the resistivity curves suggestive of electronic transitions. La_3TiSb_5, Ce_3TiSb_5, and possibly Nd_3TiSb_5 undergo transitions to a superconducting state below ~4 K. Support for the existence of a superconducting phase is also provided by onset of diamagnetism in the magnetization behavior below T_C. Extended Hückel band structure calculations disclose strongly anisotropic electrical conductivity, reflecting the one-dimensional character of covalent bonding within the structure, and reveal the presence of narrow Ti-based bands close to the Fermi level.

Introduction

The series of ternary rare-earth early-transition-metal antimonides RE_3MSb_5 (RE = La, Ce, Pr, Nd, Sm; M = Ti, Zr, Hf, Nb) has been reported, with the structures of La_3TiSb_5, La_3ZrSb_5, and La_3HfSb_5 determined from single crystals.[1,2] These compounds adopt a structure with a strongly one-dimensional character, consisting of isolated chains of face-sharing MSb_6 octahedra and linear skewers of Sb atoms that are separated by RE atoms (Figure 1). Compounds containing isolated face-sharing octahedral chains are well-known in the chalcogenides and halides, and are frequently prone to electronic phase transitions associated with the inherent low-dimensionality of their structures.[3,4] In RE_3MSb_5, magnetic properties could be influenced by the presence of moments originating from both the rare-earth and transition metal, and electrical properties could be influenced by the degree of orbital overlap within and between chains. Recent neutron diffraction studies on the isostructural ternary uranium compounds U_3TiGe_5 and U_3TiSn_5 revealed unusual magnetic behavior involving ferromagnetic ordering along the chain axis and antiferromagnetic ordering perpendicular to it.[5] One family of the rare-earth compounds, RE_3TiSb_5, was chosen for the present investigation. Their magnetic and transport properties were measured, and single-crystal X-ray structures were determined for all members so that detailed band structure calculations could be carried out.

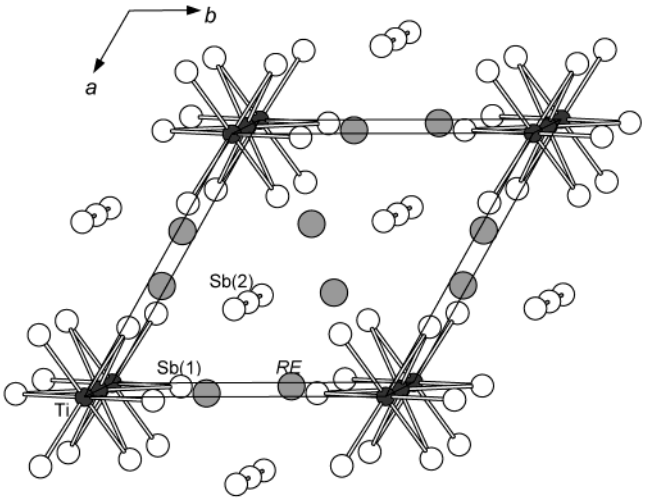

Figure 1. Structure of RE_3TiSb_5 (RE = La, Ce, Pr, Nd, Sm) viewed down the c axis. The large lightly shaded circles are RE atoms, the small solid circles are Ti atoms, and the medium open circles are Sb atoms.

Experimental Section

Synthesis. Starting materials were elemental powders (La, Ce, Pr, Nd, Sm, 99.9%, Alfa-Aesar; Ti, 99.98%, Cerac; Sb, 99.998%, Aldrich; Sn, 99.8%, Cerac). Stoichiometric mixtures of the elements (total weight 0.250 g) in the presence of a Sn flux (0.5 g) were heated in evacuated fused-silica tubes (5-cm length; 10-mm i.d.) at 570 °C for 1 day and 950 °C for 2 days. While hot, the tubes were immediately centrifuged to remove the Sn flux. The remaining mass was treated with 6 M HCl to dissolve any traces of Sn. Transport measurements were made on single crystals whose compositions were verified by EDX analyses on a Hitachi S-2700 scanning electron microscope. Magnetic measurements were made on ground samples whose purities were checked by powder X-ray diffraction on an Enraf-Nonius FR552 Guinier camera (Cu Kα radiation; Si standard). It is difficult to obtain completely pure products in the bulk,

* To whom correspondence should be addressed. Telephone: (780) 492-5592. Fax: (780) 492-8231. E-mail: arthur.mar@ualberta.ca.

(1) Bolloré, G.; Ferguson, M. J.; Hushagen, R. W.; Mar, A. *Chem. Mater.* **1995**, *7*, 2229.
(2) Ferguson, M. J.; Hushagen, R. W.; Mar, A. *J. Alloys Compd.* **1997**, *249*, 191.
(3) *Theoretical Aspects of Band Structures and Electronic Properties of Pseudo-One-Dimensional Solids*; Kanimura, H., Ed.; Physics and Chemistry of Materials with Low-Dimensional Structures, Series B; D. Reidel: Dordrecht, The Netherlands, 1985.
(4) Whangbo, M.-H.; Foshee, M. J.; Hoffmann, R. *Inorg. Chem.* **1980**, *19*, 1723.
(5) Boulet, P.; Gross, G. M.; André, G.; Bourée, F.; Noël, H. *J. Solid State Chem.* **1999**, *144*, 311.

10.1021/cm020731t CCC: $22.00
Published on Web 10/31/2002

Table 1. Crystallographic Data for RE_3TiSb_5 (RE = Ce, Pr, Nd, Sm)[a]

	Ce_3TiSb_5	Pr_3TiSb_5	Nd_3TiSb_5	Sm_3TiSb_5
fw	1077.01	1079.38	1089.37	1107.70
a (Å)	9.4277(4)	9.3835(2)	9.3517(3)	9.2758(3)
c (Å)	6.2316(3)	6.2156(2)	6.1976(2)	6.1581(2)
V (Å^3)	479.67(4)	473.96(2)	469.39(3)	458.86(3)
ρ_{calcd} (g cm^{-3})	7.457	7.563	7.708	8.017
μ (Mo Kα) (cm^{-1})	284.61	298.17	311.30	340.67
$R(F)$ for $F_o^2 > 2\sigma(F_o^2)$[b]	0.039	0.020	0.023	0.042
$R_w(F_o^2)$[c]	0.077	0.042	0.057	0.075

[a] For all structures listed, space group is D_{6h}^3–$P6_3/mcm$ (No. 193), $Z = 2$, $T = 22$ °C, and $\lambda = 0.71073$ Å. [b] $R(F) = \sum||F_o| - |F_c||/\sum|F_o|$. [c] $R_w(F_o^2) = [\sum[w(F_o^2 - F_c^2)^2]/\sum wF_o^4]^{1/2}$; $w^{-1} = [\sigma^2(F_o^2) + (ap)^2 + (bp)]$ where $p = [\max(F_o^2,0) + 2F_c^2]/3$.

Table 2. Positional and Equivalent Isotropic Displacement Parameters for RE_3TiSb_5 (RE = Ce, Pr, Nd, Sm)

	Ce_3TiSb_5	Pr_3TiSb_5	Nd_3TiSb_5	Sm_3TiSb_5
RE at 6g (x, 0, 1/4)				
x	0.61740(8)	0.61738(5)	0.61757(5)	0.61727(9)
U_{eq} (Å^2)[a]	0.0081(2)	0.0097(1)	0.0104(2)	0.0089(2)
Ti at 2b (0, 0, 0)				
U_{eq} (Å^2)[a]	0.0081(8)	0.0094(4)	0.0102(5)	0.0079(8)
Sb(1) at 6g (x, 0, 1/4)				
x	0.25307(10)	0.25426(6)	0.25545(7)	0.25715(11)
U_{eq} (Å^2)[a]	0.0078(2)	0.0092(1)	0.0099(2)	0.0082(2)
Sb(2) at 4d (1/3, 2/3, 0)				
U_{eq} (Å^2)[a]	0.0080(3)	0.0096(2)	0.0103(2)	0.0082(3)

[a] U_{eq} is defined as one-third of the trace of the orthogonalized $\mathbf{U}_{ij}$ tensor.

Table 3. Selected Interatomic Distances (Å) in RE_3TiSb_5 (RE = La, Ce, Pr, Nd, Sm)

	La_3TiSb_5[a]	Ce_3TiSb_5	Pr_3TiSb_5	Nd_3TiSb_5	Sm_3TiSb_5
RE–Sb(1) (×2)	3.2064(8)	3.1776(6)	3.1649(4)	3.1549(4)	3.1345(6)
RE–Sb(2) (×4)	3.3598(4)	3.3255(3)	3.3114(2)	3.3011(2)	3.2747(3)
RE–Sb(1) (×2)	3.3815(8)	3.3466(5)	3.3330(3)	3.3185(3)	3.2920(5)
RE–Sb(1)	3.496(1)	3.4348(12)	3.4074(7)	3.3865(8)	3.3403(13)
RE–RE (×2)	3.858(1)	3.8221(9)	3.8094(5)	3.7997(6)	3.7700(9)
Ti–Sb(1) (×6)	2.859(1)	2.8495(8)	2.8472(5)	2.8473(6)	2.8390(9)
Ti–Ti (×2)	3.1400(5)	3.1158(2)	3.1078(1)	3.0988(1)	3.0790(1)
Sb(2)–Sb(2) (×2)	3.1400(5)	3.1158(2)	3.1078(1)	3.0988(1)	3.0790(1)

[a] At −60 °C.[1]

presumably because of problems in incongruent melting behavior.

Structure Determination. The structure of La_3TiSb_5 has been determined previously from single-crystal X-ray diffraction data, but only cell parameters have been obtained for the remaining RE_3TiSb_5 members (RE = Ce, Pr, Nd, Sm).[1] In anticipation of a comparative study of their band structures, single-crystal diffraction data were collected. Intensity data were collected on a Bruker Platform/SMART 1000 CCD diffractometer at 22 °C using ω scans (0.2°). Crystal data are given in Table 1. Calculations were carried out with use of the SHELXTL (version 5.1) package.[6] Face-indexed numerical absorption corrections were applied. The centrosymmetric space group $P6_3/mcm$ was chosen and initial atomic positions were taken from the structure of La_3TiSb_5. Refinements proceeded in a straightforward manner, and revealed no evidence for partial occupancy of sites. The difference electron density maps are featureless after the final refinements. Final values of the positional and displacement parameters are given in Table 2, interatomic distances are listed in Table 3, and further data in the form of a CIF are available as Supporting Information.

Transport Measurements. Standard four-probe techniques were applied on a Quantum Design PPMS system equipped with an ac transport controller (model 7100). Electrical resistivities from 2 to 300 K were measured on needle-shaped single crystals, typically 0.05−0.10 mm wide and 0.5−0.8 mm long, that were previously screened by EDX analyses. A current of 0.10 mA and 16 Hz was applied parallel to the needle axis (crystallographic c axis). Magnetoresistance data were obtained under zero-field-cooled conditions with the needle axis perpendicular to the applied field. All measurements were repeated at least twice on separate samples. Superconducting critical temperatures were determined at the point at which the resistivity drops to 90% of the normal value.

Magnetic Measurements. Magnetic data were obtained on ground samples placed in gelcap sample holders with a Quantum Design 9T-PPMS dc magnetometer/ac susceptometer between 2 and 300 K. A driving amplitude of 1 Oe and frequencies between 1000 and 5000 Hz were used in ac magnetic susceptibility measurements. In dc magnetic measurements, the susceptibility was corrected for contributions for the holder diamagnetism and the underlying sample diamagnetism using these values (emu mol^{-1}): RE, -20×10^{-6}; Ti, -15×10^{-6}; Sb, -15×10^{-6}. Complete magnetic characterization was plagued by difficulties in synthesis of phase-pure bulk samples. Samples were typically 70−90% pure, as gauged by powder X-ray diffraction. The major impurity is elemental Sb, which is not superconducting under ambient pressures; in all cases, elemental Sn, which is superconducting at 3.722 K,[7] was not detectable.

Band Structure. One-electron tight-binding extended Hückel band structure calculations were performed on the $[TiSb_5]^{9-}$ substructure of RE_3TiSb_5 members, with use of the EHMACC suite of programs.[8,9] Extended Hückel parameters were taken from literature values and are listed in Table 4.[10] Properties were extracted from the band structure using 50 k points in the irreducible portion of the Brillouin zone.

(6) Sheldrick, G. M. *SHELXTL*, version 5.1; Bruker Analytical X-ray Systems, Inc.: Madison, WI, 1997.

(7) Roberts, B. W. *Properties of Selected Superconductive Materials*; U.S. Government Printing Office: Washington, DC, 1978.

(8) Whangbo, M.-H.; Hoffmann, R. *J. Am. Chem. Soc.* **1978**, *100*, 6093.

(9) Hoffmann, R. *Solids and Surfaces: A Chemist's View of Bonding in Extended Structures*; VCH Publishers: New York, 1988.

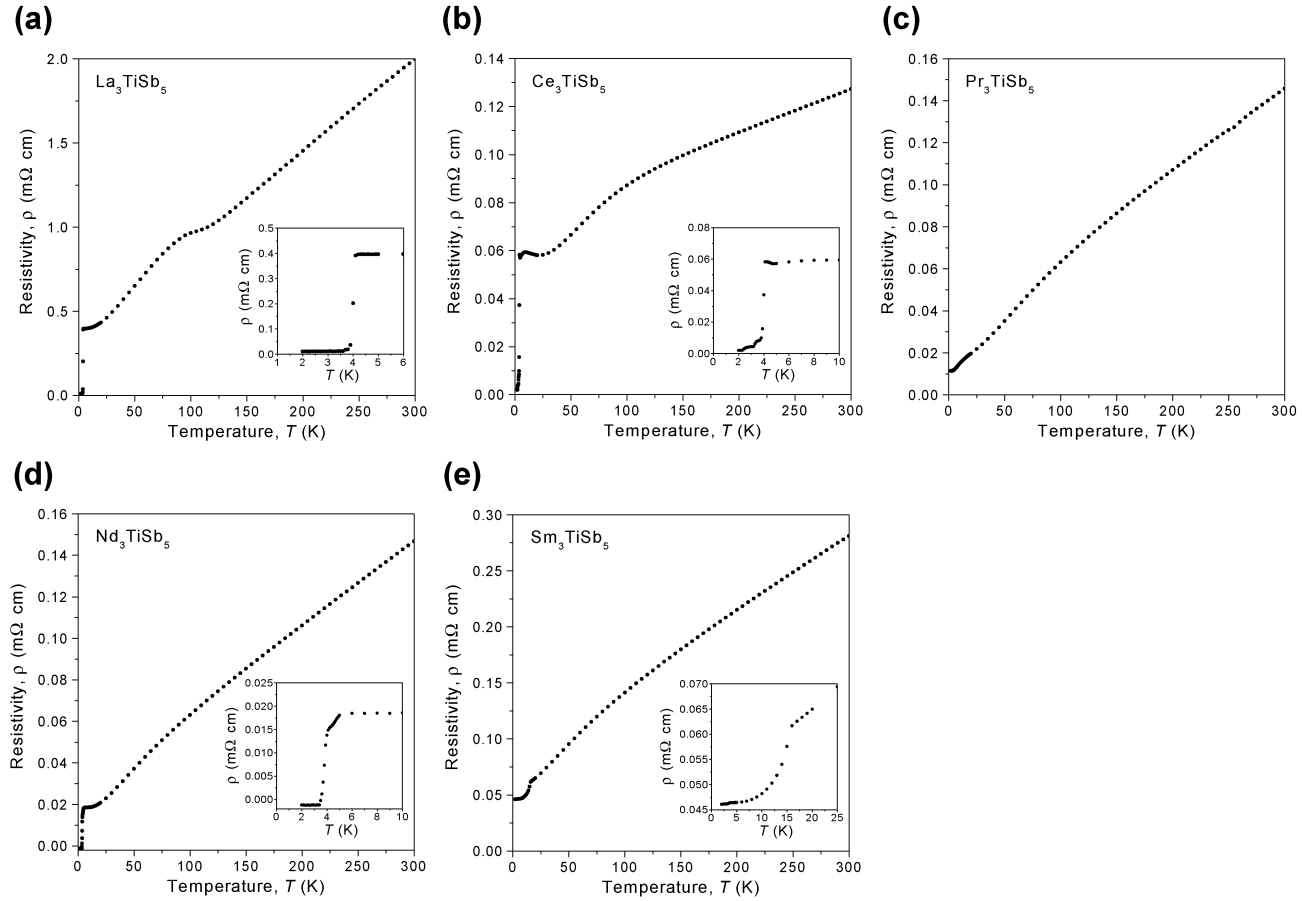

Figure 2. Zero-field electrical resistivity of single crystals of RE_3TiSb_5 (RE = (a) La, (b) Ce, (c) Pr, (d) Nd, (e) Sm) measured along the *c* axis between 2 and 300 K. Insets show low-temperature behavior.

Table 4. Extended Hückel Parameters

atom	orbital	H_{ii} (eV)	ζ_{i1}	c_1	ζ_{i2}	c_2
Ti	4s	−8.48	1.50			
	4p	−4.60	1.50			
	3d	−9.26	4.55	0.4391	1.60	0.7397
Sb	5s	−18.8	2.323			
	5p	−11.7	1.999			

Results and Discussion

Structure. Substitution of the rare earth in RE_3TiSb_5 does not contract the structure uniformly. Examination of interatomic distances and angles reveals that maintaining a reasonable Ti−Sb(1) bond length within the face-sharing octahedral chains is most important. The Ti−Sb(1) distances remain relatively constant while the Ti−Ti and Sb(2)−Sb(2) contacts, parallel to the *c*-direction, gradually decrease upon substitution of a smaller *RE*. Consequently, the octahedral chains become increasingly distorted, flattening along the *c*-direction, as revealed by the deviation from ideal octahedral angles on going from La_3TiSb_5 (87.27(2)° and 92.73(2)°) to Sm_3TiSb_5 (86.62(2)° and 93.38(2)°). The shortest *RE*−*RE* contacts (∼3.8 Å) occur along zigzag chains running parallel to the *c*-axis; the next-closest distances are over ∼4.8 Å. As discussed elsewhere, the Sb(2)−Sb(2) distances of ∼3.1 Å within the linear skewers are suggestive of weak bonding interactions, modeled to a first approximation as one-electron bonds.[11] Applying the Zintl concept and assuming that full electron transfer takes place, the formulation $(La^{3+})_3(Ti^{4+})(Sb(1)^{3-})_3(Sb(2)^{2-})_2$ is obtained. However, it is unclear whether the Ti−Ti distances, also of ∼3.1 Å, indicate bonding, in which case the oxidation state assignment of Ti^{4+} would have to be modified. Nevertheless, the expectation based on inspection of the crystal structure is that the electronic properties will be highly anisotropic.

Transport Properties. Table 5 summarizes some of the electrical and magnetic properties of RE_3TiSb_5. Figure 2 shows the resistivity as a function of temperature for RE_3TiSb_5 members measured along the *c* axis. All compounds display metallic behavior, with resistivities generally decreasing from room temperature down, but with prominent transitions occurring at low temperatures. In the high-temperature regime (>50 K), La_3TiSb_5 shows a change in slope at 120 and 85 K. This feature occurs reproducibly in all samples of La_3TiSb_5 examined. In the other RE_3TiSb_5 members, the resistivity plots also show a curvature that becomes gradually less pronounced on proceeding to Sm_3TiSb_5. These transitions are reminiscent of behavior observed in niobium and tantalum trichalcogenides,[3] but a definitive proposal for their origin is deferred until more detailed variable-temperature structural studies become available.

In the low-temperature regime (<50 K), some striking transitions are observed. La_3TiSb_5, Ce_3TiSb_5, and Nd_3-

(10) Kleinke, H. *J. Am. Chem. Soc.* **2000**, *122*, 853.

(11) Papoian, G. A.; Hoffmann, R. *Angew. Chem., Int. Ed.* **2000**, *39*, 2408.

Table 5. Summary of Resistivity and Magnetism Data for RE_3TiSb_5

	La_3TiSb_5	Ce_3TiSb_5	Pr_3TiSb_5	Nd_3TiSb_5	Sm_3TiSb_5
$\rho_{300\ K}$ (Ω cm)	2.0×10^{-3}	1.3×10^{-4}	1.5×10^{-4}	1.5×10^{-4}	2.8×10^{-4}
$\rho_{300\ K}/\rho_{5\ K}$	5.0	2.3	12	8.2	6.1
T_C (K)	4.1[a]/4.0[b]	4.0[a]/3.9[b]		3.7[a]	
H_{C1}, H_{C2} (2 K) (Oe)	70, 370	70, 150			

[a] Determined from ρ vs T plot. [b] Determined from χ'_{ac} vs T plot.

$TiSb_5$ undergo drops to zero resistivity (within instrumental error) below T_C = 4.1, 4.0, and 3.7 K, respectively. Ce_3TiSb_5 also shows a local minimum in the resistivity curve at 25 K that is similar in behavior to that observed in other Ce-containing Kondo systems.[12,13] Sm_3TiSb_5 displays an abrupt decrease in resistivity at 16 K, which is attributed to the occurrence of magnetic ordering of the Sm moments.

Magnetism and Magnetoresistance. All compounds show a positive magnetization at 2 K under applied fields greater than 500 Oe and no frequency dependence in the ac magnetic susceptibility from 1 to 5 kHz. For La_3TiSb_5 and Ce_3TiSb_5, the magnetic data are consistent with the single-crystal electrical resistivity data showing the occurrence of superconducting transitions, and are reported in detail herein.

In La_3TiSb_5, the transition to zero resistivity shifts to lower temperatures as a higher magnetic field is applied (Figure 3a). Evidence for superconductivity is further provided by the ac magnetic susceptibility measurements, which reveal both diamagnetic shielding (under zero-field-cooled conditions) and the Meissner effect (under field-cooled conditions) (Figure 3b). The resistivity and magnetic susceptibility data establish T_C at 4.0 K. At 2 K, the dc magnetization curve (M vs H) reveals a profile characteristic of a type-II superconductor with critical fields of H_{C1} = 70 Oe and H_{C2} = 370 Oe (Figure 3c).

Although also a superconductor, Ce_3TiSb_5 is more complicated owing to the presence of a 4f electron in nominally Ce^{3+}. As in the La member, the resistivity shows a depression of T_C with greater applied magnetic fields (Figure 4a). The effective moment in Ce_3TiSb_5 at 300 K is 2.4 μ_B per Ce ion, close to that expected for Ce^{3+} (2.54 μ_B), and the θ_W value extracted from a fit of the dc magnetic susceptibility data at high temperature (not shown) to the Curie−Weiss law is −36 K. The negative χ'_{ac} values seen in the ac magnetic susceptibility data further support the occurrence of superconductivity with a T_C of 3.9 K (Figure 4b). At 2 K, the negative magnetization profile at very low fields (inset of Figure 4c) substantiates Ce_3TiSb_5 as a type-II superconductor with critical fields of H_{C1} = 75 Oe and H_{C2} = 150 Oe. Above 150 Oe, the magnetization becomes positive and displays two inflection points at 7600 and 16 000 Oe (Figure 4c). Even under high-field conditions, up to H = 9 T, the magnetization has not reached saturation. These field-induced transitions observed below 3.9 K suggest the presence of coexisting superconducting and magnetically ordered phases. At 2 K, the upper critical field of 150 Oe separates the superconducting from the magnetic regimes, but we have not determined the temperature dependence of this critical field. The nature of the magnetic phase remains an open question until further magnetic data on samples of greater purity or on large single crystals are available, preferably from neutron diffraction studies.

The magnetic data for Pr_3TiSb_5 and Nd_3TiSb_5 were deemed unreliable because not all impurities could be identified or significant amounts of other magnetic phases (such as $PrSb_2$) were observed. The resistivity of a single crystal of Nd_3TiSb_5 also shows a gradual decrease in T_C with greater applied fields similar to the behavior seen in La_3TiSb_5 and Ce_3TiSb_5 (Figure 5). Although evidence from the magnetic data supporting a superconducting phase in Nd_3TiSb_5 is unavailable, the similar behavior observed for the other members of this series lends credibility to the proposal that Nd_3TiSb_5 is also a superconductor below 3.7 K.

Although the Sm_3TiSb_5 sample was about 70% pure, the dc magnetic susceptibility vs temperature plot (Figure 6) reveals an anomaly at the same temperature (16 K) at which an abrupt transition occurs in the resistivity vs temperature plot (Figure 2e). The magnetic susceptibility does not obey the Curie−Weiss law and the isothermal magnetization at 2 K displays only positive values and a linear dependence with field (not shown). A possible interpretation is that the Sm 4f electrons are interacting with the conduction electrons to form a magnetic ground state that is favored over a superconducting phase, and loss of spin-disorder scattering accounts for the abrupt decrease in resistivity below 16 K.

Band Structure. Calculations were carried out on the $[TiSb_5]^{9-}$ substructure of RE_3TiSb_5 compounds to confirm their metallic conductivity and to ascertain the extent of Ti−Ti and Sb−Sb bonding. Because it is a one-electron method, an extended Hückel calculation cannot account for the magnetic properties of these compounds, which arise primarily from the rare-earth ions that are neglected for consideration. In any case, reliable Hückel parameters for many rare-earth elements are unavailable. Although the $[TiSb_5]^{9-}$ substructure can be considered as the superposition of independent chains of composition $[TiSb_3]^{5-}$ and $[Sb_2]$,$^{4-}$ the rare-earth atoms can nevertheless be important if they participate in some degree of covalent bonding, effectively coupling these chains together.

The band dispersion for La_3TiSb_5 plotted along special symmetry lines within the Brillouin zone is shown in Figure 7. The most striking feature is that four disperse bands cross the Fermi level along ΓA, parallel to the axis of the $[TiSb_3]^{5-}$ and $[Sb_2]^{4-}$ chains, and that none crosses the Fermi level along the other directions. The two widest bands along ΓA are associated with orbital interactions involving π-overlap of Ti d orbitals having a z-component with Sb(1) s−p hybrid orbitals within the $[TiSb_3]$ octahedral chains, as well as σ-overlap of Sb(2) p_z orbitals within the linear Sb skewers. The two

(12) Chevalier, B.; Etourneau, J. *J. Mater. Chem.* **1999**, *9*, 1789.
(13) Gordon, R. A.; DiSalvo, F. J.; Pöttgen, R. *J. Alloys Compd.* **1995**, *228*, 16.

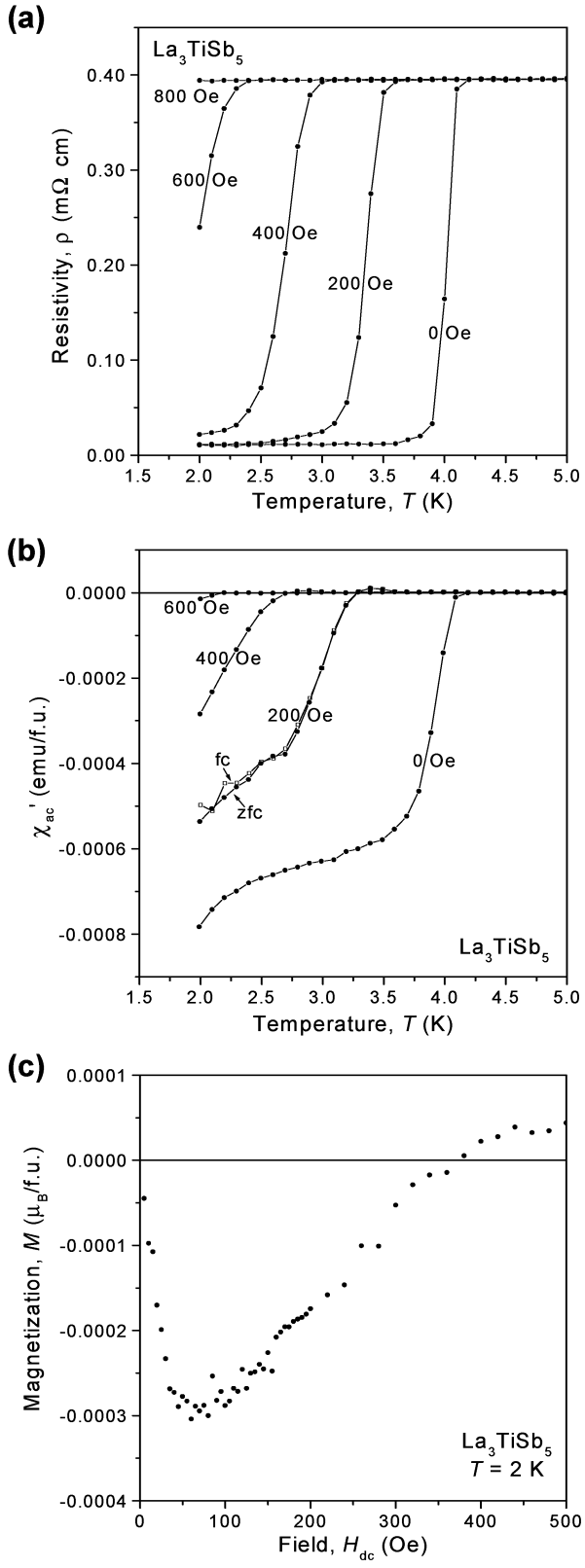

Figure 3. (a) Field dependence of single-crystal electrical resistivity, (b) temperature dependence of zero-field-cooled ac magnetic susceptibility under various applied fields (and an additional field-cooled run at 200 Oe), and (c) isothermal magnetization at 2 K for La_3TiSb_5. Lines shown are included only to guide the eye.

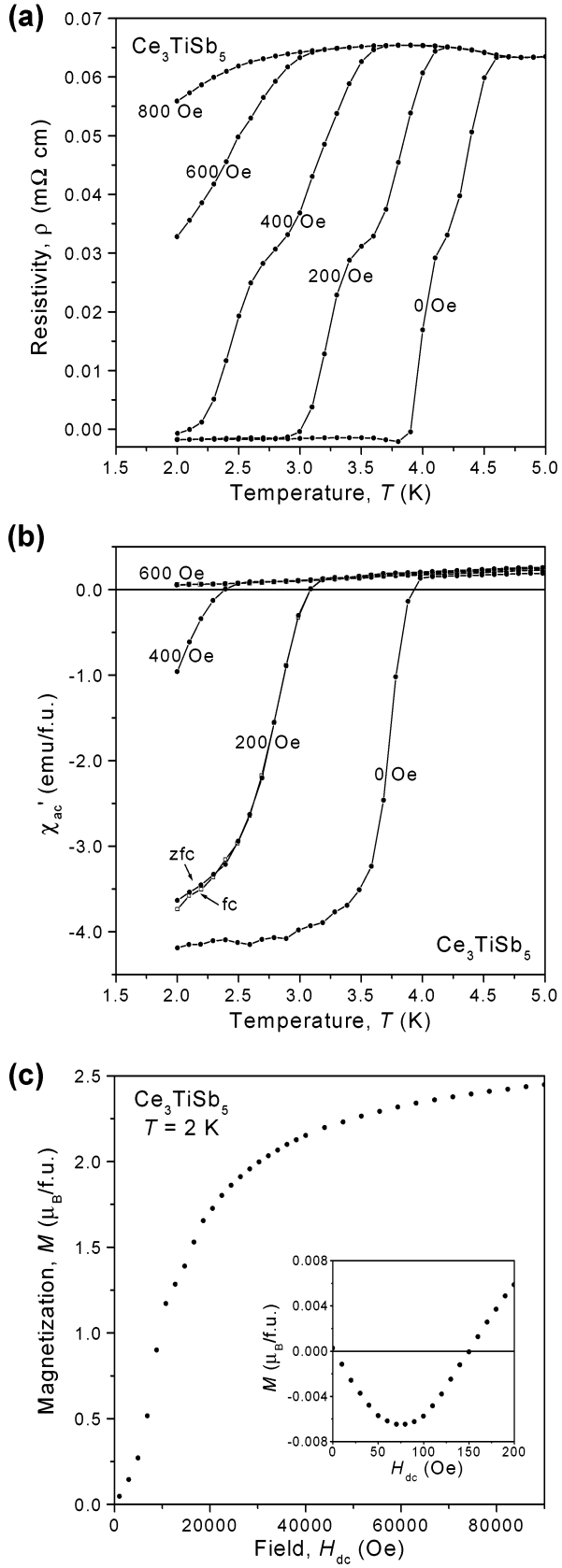

Figure 4. (a) Field dependence of single-crystal electrical resistivity, (b) temperature dependence of zero-field-cooled ac magnetic susceptibility under various applied fields (and an additional field-cooled run at 200 Oe), and (c) isothermal magnetization at 2 K for Ce_3TiSb_5. Lines shown are included only to guide the eye.

narrower bands involve weak overlap of Ti d_z^2 orbitals mediated to a small extent by Sb(1) p_z orbitals. Along other directions, these bands show little or no dispersion, as expected given that the closest separation

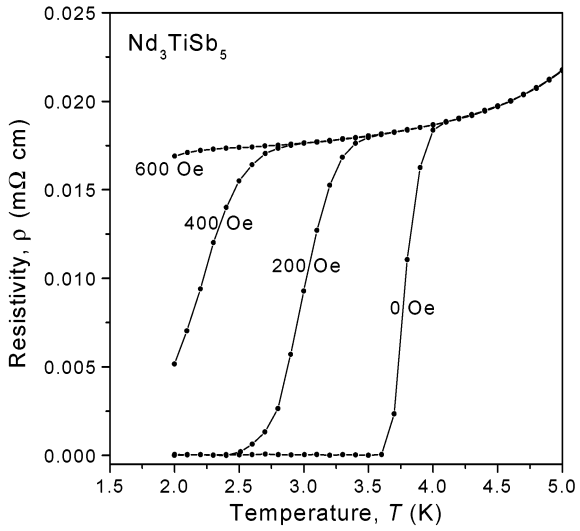

Figure 5. Field dependence of single-crystal electrical resistivity for Nd_3TiSb_5.

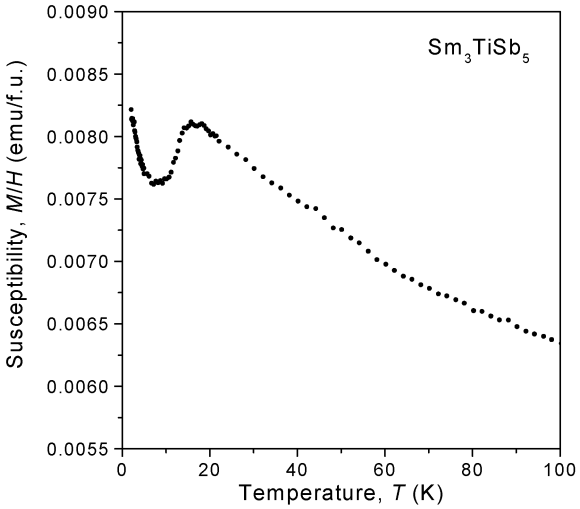

Figure 6. Magnetic susceptibility (M/H) of Sm_3TiSb_5 under an applied field of 1.0 T.

between $[TiSb_3]$ and $[Sb_2]$ chains is nearly 6 Å. Thus, La_3TiSb_5 can be regarded as a highly anisotropic metal with conduction along the needle axis being much greater than that perpendicular to it.

The Fermi level falls in a region of very high density of states (DOS), as shown in Figure 8a, just below a large maximum in the curve. In this region, the states are dominated by contributions from Ti d orbitals. The occurrence of both narrow and wide bands near the Fermi level is often touted as a signature for superconductivity,[14,15] although this is not a sufficient condition; further analysis of the electron−phonon coupling processes is required.[16−18] In the case of RE_3TiSb_5, the position of the Fermi level would be quite sensitive to minor changes arising from small contractions in the structure or involvement of the rare-earth atoms in covalent bonding.

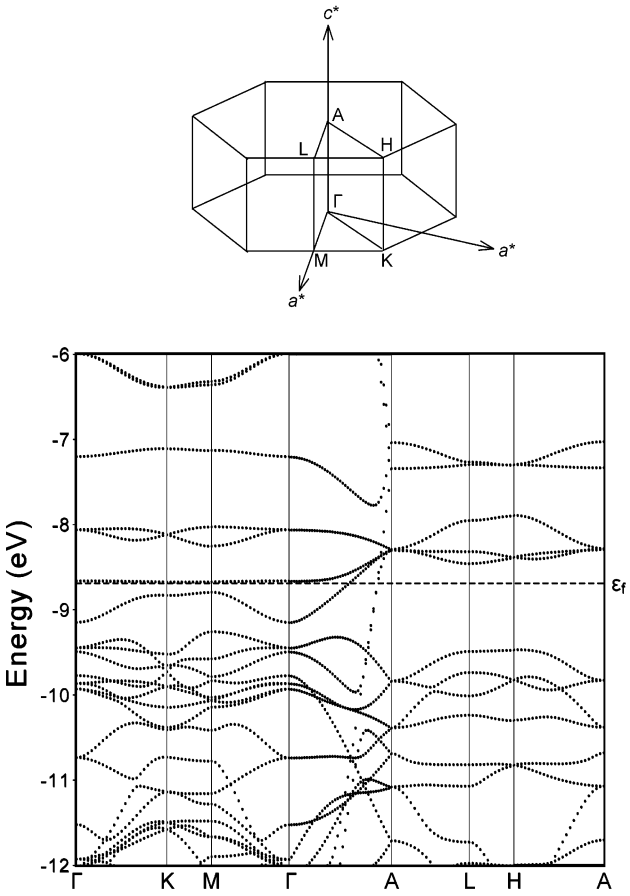

Figure 7. Band dispersion curves along special symmetry lines for the $[TiSb_5]^{9-}$ substructure in La_3TiSb_5. The dashed horizontal line marks the Fermi level ($\varepsilon_f = -8.71$ eV). A representation of the hexagonal Brillouin zone is shown with the irreducible wedge outlined.

Crystal orbital overlap population (COOP) curves are plotted in Figure 8b−d. The Ti−Sb bonding is optimized with all bonding states and no antibonding states occupied, resulting in an integrated overlap population of 0.505, typical of a strong single-bond interaction. For the longer 3.140 Å Sb−Sb and Ti−Ti contacts, some antibonding states are filled. The overlap population for the Sb−Sb contact is 0.227, roughly half of that expected for a single bond and consistent with the usual description of these distances in linear Sb chains as "one-electron" bonds. For the Ti−Ti contact, the overlap population is 0.078, which is small but emphatically positive, suggesting some degree of metal−metal bonding.

Assuming that the *RE* atoms play no role in mediating electronic conduction, similar band structure calculations on the $[TiSb_5]^{9-}$ substructure in the other members of the RE_3TiSb_5 series should reveal the effect of contracting the structure. Table 6 summarizes the results. Although the changes are small, the bands generally become more disperse, and to maintain the same electron count the Fermi level rises slightly. The Ti−Sb bonding remains of constant strength because the bond length does not change significantly. However, there is a noticeable transfer of electron density from the Sb atoms to the Ti atoms, as seen in the trend in Mulliken charges. The bonding is already quite weak for the Sb−Sb and more so for the Ti−Ti contacts, but

(14) Felser, C. *J. Solid State Chem.* **2001**, *160*, 93.
(15) Simon, A. *Angew. Chem., Int. Ed. Engl.* **1997**, *36*, 1788.
(16) Deng, S.; Simon, A.; Köhler, J. *Angew. Chem., Int. Ed.* **1998**, *37*, 640.
(17) Deng, S.; Simon, A.; Köhler, J. *Solid State Sci.* **2000**, *2*, 31.
(18) Deng, S.; Simon, A.; Köhler, J. *J. Phys. Chem. Solids* **2001**, *62*, 1441.

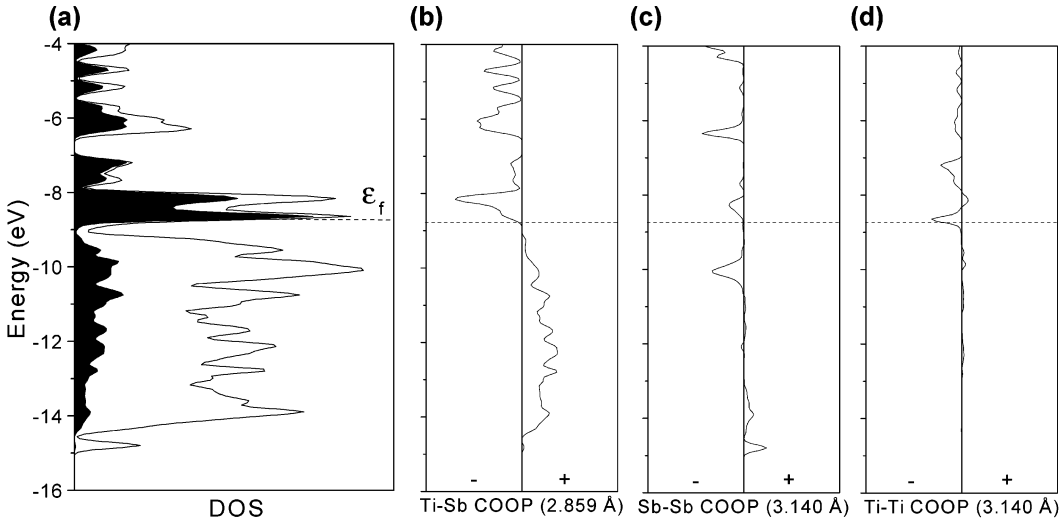

Figure 8. (a) Density of states (DOS) (with the Ti projection shown by the filled area; what remains of the DOS is the Sb projection) and crystal orbital overlap population (COOP) curves for the (b) Ti−Sb, (c) Sb−Sb, and (d) Ti−Ti contacts in the $[TiSb_5]^{9-}$ substructure in La_3TiSb_5. The dashed horizontal line marks the Fermi level ($\varepsilon_f = -8.71$ eV).

Table 6. Mulliken Charges and Integrated Overlap Populations for $[TiSb_5]^{9-}$ Substructure in RE_3TiSb_5

	La_3TiSb_5	Ce_3TiSb_5	Pr_3TiSb_5	Nd_3TiSb_5	Sm_3TiSb_5
ε_f (eV)	−8.71	−8.65	−8.64	−8.62	−8.59
Mulliken charge					
Ti	−0.39	−0.65	−0.80	−0.87	−1.18
Sb	−1.72	−1.68	−1.64	−1.61	−1.56
overlap population					
Ti−Sb	0.505	0.506	0.506	0.505	0.506
Sb−Sb	0.227	0.229	0.220	0.231	0.232
Ti−Ti	0.078	0.077	0.074	0.077	0.067

this electron-transfer entails a minor strengthening of the Sb−Sb bonds and minor weakening of the Ti−Ti bonds on going from La_3TiSb_5 to Sm_3TiSb_5.

The Ti d-bands are partially occupied, ranging from $d^{3.2}$ in La_3TiSb_5 to $d^{4.0}$ in Sm_3TiSb_5. However, there are narrow bands available very close to the Fermi level (Figure 7) and their relative positions would be sensitive to temperature, among other factors. This suggests that any of the RE_3TiSb_5 compounds are subject to electronic instability, and may account for the transitions in the electrical resistivity plots (Figure 2). Opposing the tendency for structural distortions that may ensue from these electronic transitions would be the impetus to maintain strong Ti−Sb bonds within the face-sharing octahedral chains.

Conclusion

The RE_3TiSb_5 compounds are metallic with the La, Ce, and probably Nd members being superconducting. The band structures of the $[TiSb_5]^{9-}$ substructures are similar in all compounds, suggesting that the occurrence of a superconductive phase is highly sensitive to the nature of the rare earth or the cell contraction. The magnetic data for powder samples of the La, Ce, and Sm members are consistent with the electrical resistivity data for single crystals; in particular, the critical temperatures determined from the two types of data are in agreement for the superconducting La and Ce members. In Ce_3TiSb_5, the observation of field-induced transitions suggests the occurrence of both superconducting and ordered magnetic phases below T_C. There is evidence for weak Ti−Ti bonding as one possible source for electronic instability. Examination of other RE_3MSb_5 (M = Zr, Hf, Nb) compounds, where $M-M$ interactions are expected to be stronger, would therefore be of great interest.

Acknowledgment. The Natural Sciences and Engineering Research Council of Canada and the University of Alberta supported this work. We thank Dr. Robert McDonald (Faculty Service Officer, X-ray Crystallography Laboratory) for the X-ray data collection, and Ms. Christina Barker (Department of Chemical and Materials Engineering) and Mr. George Braybrook (Department of Earth and Atmospheric Sciences) for assistance with the EDX analyses.

Supporting Information Available: An X-ray crystallographic file for the structures of RE_3TiSb_5 (RE = Ce, Pr, Nd, Sm) (CIF). This material is available free of charge via the Internet at http://pubs.acs.org.

CM020731T